Environmental Science and Pollution Research (2022) 29:61397–61411
https://doi.org/10.1007/s11356-022-20223-z

RESEARCH ARTICLE

# Multi-isotopes revealing the coastal river anthropogenic pollutants and natural material flux to ocean: Sr, C, N, S, and O isotope study

**Shitong Zhang[1] · Guilin Han[1] · Jie Zeng[1] · Man Liu[1] · Xiaoqiang Li[1] · Jinke Liu[1]**

Received: 30 June 2021 / Accepted: 8 April 2022 / Published online: 20 April 2022


## Abstract

Coastal river exports massive terrestrial materials to the adjacent marine environment with information about chemical weathering, providing critical insights on riverine flux and the potential impact on marine ecosystem. In this study, the preliminary data of dissolved strontium (Sr) and $^{87}Sr/^{86}Sr$ in a typical coastal river in southeastern China were collected along with hydrochemistry and C, N, S, and O isotopes to discriminate the source of terrestrial weathering and the riverine flux. Sr concentrations exhibited a range of 0.084 ~ 1.307 μmol $L^{-1}$, and $^{87}Sr/^{86}Sr$ values ranged 0.7089 ~ 0.7164. The total cationic charge ($TZ^+$) ranged 0.2 ~ 11.7 meq $L^{-1}$ with the predominant $Ca^{2+}$ which accounted for > 50% of $TZ^+$, while the anions were dominated by $HCO_3^-$. The extremely high $Na^+$ and $Cl^-$ near the estuary indicated seawater mixing in such a coastal river. $\delta^{13}C$-DIC, $\delta^{15}N$-$NO_3^-$, $\delta^{18}O$-$NO_3^-$, and $\delta^{34}S$-$SO_4^{2-}$ of river water ranged − 24.1‰ ~ − 9.2‰, 0.3‰ ~ 22.7‰, − 2.1‰ ~ 21.4‰, and − 9.3‰ ~ 18.0‰, respectively. $\delta^{13}C$ enhanced correspondingly to decreased $\delta^{34}S$, confirming the attendance of $H_2SO_4$ in carbonate weathering. Most $\delta^{18}O$ values exhibited within ± 10‰, indicating the dominant nitrification process. $\delta^{15}N$ presented slightly negative relationship with $\delta^{13}C$ and no obvious correlation with $\delta^{34}S$, indicating relatively limited impact of denitrification. The depleted $\delta^{13}C$ and $\delta^{15}N$ may be attributed to carbonate dissolution with nitric acids and the oxidation of organic matters into C and N pools. Quantitative analysis revealed that silicate weathering accounts for 79% of total dissolved Sr, indicating the dominant weathering process. The estimated monthly flux of dissolved Sr to the East China Sea was 138.1 tons, demonstrating an potential impact on seawater Sr isotope evolution. Overall, the investigations of multi-isotopes revealed the enhancement of weathering rates and the consequently depleted $CO_2$ consumption, which further proved the involvement of strong acids ($H_2SO_4$ and $HNO_3$). This study provides scientific insight in terrestrial weathering and anthropogenic impact of a typical coastal watershed and may orient the management of environmental issues related to coastal ecosystems.

**Keywords** Jiulongjiang River · Coastal ecosystem · Chemical weathering · Riverine flux · Strong acids

## Introduction

As an essential connection between land and ocean, coastal rivers export terrestrial materials from terrestrial weathering to marine environment, which accordingly influence the coastal carbon cycle and $CO_2$ consumption (Palmer and Edmond 1989, 1992; Capo et al. 1998; Ding et al. 2017). Chemical weathering leads a vital role in regulating ion composition and coastal river outflows (Gaillardet et al. 1999; Fan and Huang 2008; Cao et al. 2020; Mora et al. 2020) and dominates the $CO_2$ level through geological times which makes great contribution to coastal and marine carbon cycle (Krishnaswami et al. 1992; Wang et al. 2012; Bertrand et al. 2022). Therefore, investigations on terrestrial weathering and the quantification of source contributions to coastal riverine solutes have been widely conducted throughout the world (Roy et al. 1999; Gaillardet et al. 2018; Chen et al. 2020; Boral et al. 2021), providing us with fundamental understanding of the dynamic weathering processes occurred in coastal riverine environment (Tripathy and Singh 2010) and revealing the roles of both natural and anthropogenic causes of changes in marine ecosystems.

Responsible Editor: V.V.S.S. Sarma

✉ Guilin Han
hanguilin@cugb.edu.cn

[1] Institute of Earth Sciences, China University of Geosciences (Beijing), Beijing 100083, China

Terrestrial weathering in a coastal river basin mainly depends on bedrock lithology, anthropogenic inputs, and atmospheric wet/dry deposition. Previous works have indicated that strong acids released via natural/anthropogenic inputs may also have great impact on weathering process (sulfide oxidation, nitrogen fertilizer, etc.) (Wang et al. 2012). Sr concentration and its isotope composition have been widely demonstrated to be an effective tool for fingerprinting ion sources (Liu et al. 2016), identifying weathering end-members, and estimating weathering rates and $CO_2$ consumption budget, since $^{87}Sr/^{86}Sr$ exhibit negligible variations during weathering processes (Palmer and Edmond 1989, 1992; Krishnaswami et al. 1992; Negrel et al. 1993; Capo et al. 1998; Mahlknecht et al. 2017). Strontium in riverine systems can generally be expressed as a result of chemical weathering from two end-members: One is originated from carbonate mineral dissolution with higher Sr concentration and lower $^{87}Sr/^{86}Sr$ (0.708 ~ 0.710), while the other is silicate weathering with lower Sr and higher $^{87}Sr/^{86}Sr$ (> 0.710) due to enrichment of $^{87}Sr$ (Zieliński et al. 2016; Zhang et al. 2019; Liu and Han 2020). The strontium concentration and $^{87}Sr/^{86}Sr$ were investigated thoroughly in this study to reveal the contributions of weathering agents in JLJ River basin and provide basic insights on the potential origins of dissolved Sr and riverine fluxes into the ocean.

Multi-isotope coupling has been widely applied to improve the precision of measuring and analyzing parameters of groundwater and surface water, especially those cannot be interpreted thoroughly by one single isotope (Aravena and Robertson 1998; Otero et al. 2009; Li and Ji 2016; Wu and Han 2018; Zeng and Han 2020; Zhang and Wang 2020; Torres-Martínez et al. 2021). This method is gradually adopted to the research of the large river ecosystems in the world (Li et al. 2010b; Marchina et al. 2016; Han et al. 2020), but the investigations on medium-sized coastal river basin are still relatively rare. Jiulongjiang (JLJ) River, the second largest river in Fujian Province (southeast China), is a typical middle-size subtropical river which is under the impact of coastal ecosystem. Considering the high-density regional population (more than 3.6 million) and rapid progress of urbanization within the JLJ basin (Liu et al. 2021), the dissolved materials obtained from terrestrial processes have been extensively altered throughout the river flow and finally to the East China Sea. Therefore, this change has threatened the environmental security not only in the JLJ River basin, but also in such an essential coastal ecosystem (Liu and Han 2020). Our previous work on this typical coastal region has already demonstrated the basic hydrological processes of regional water cycle under the impact of anthropogenic influence and precipitation (Yang et al. 2018; Li et al. 2019), the sources of potential weathering agents based on geological background and land use (Liu and Han 2020), and the dissolved inorganic carbon flux (Liu et al. 2019). However, the end-member contribution and sources of chemical weathering in detail under the background of both natural and anthropogenic constraints is still unclear. In such circumstances, a further investigation of multi-isotope coupling in this study could provide an explicit perspective on terrestrial weathering under human disturbance and may orient in solving environmental issues related to coastal ecosystem.

The main aims of this study are to (a) characterize the spatial distribution and variation of Sr and its isotopic compositions, (b) identify sources of dissolved Sr and its indications for weathering end-members, (c) demonstrate the role of strong acids and other weathering agents combined with hydrochemistry and multi-isotope data, and (d) estimate the Sr output flux and weathering constraints based on multi-isotopes. The results may deepen the understanding of coastal environment and the ion flux to the adjacent ocean under human perturbations.

## Materials and methods

### Study area

Jiulongjiang River (24°18′ ~ 25°88′ N, 116°78′ ~ 118°03′ E, Fig. 1), with a drainage area of 14,087 $km^2$ and water discharge of 14 $km^3$ annually, is the largest river in Fujian Province which discharges into the East China Sea (Liu and Han 2020). North River (NR, mainstream), West River (WR, main tributary), and South River (SR, main tributary) are three main channels of JLJ River. With the average temperature of 21℃, JLJ basin is dominated by subtropical oceanic monsoon climate with high rainfall amount and about 75% of water discharge in the wet season (April to September) (Liu and Han 2020). The upper reaches of the JLJ River mainly flow through mountainous areas with high vegetation coverage, relatively few human disturbances, and a mean precipitation of 2000 mm annually. Lower reaches flow through rural areas with less precipitation; that is, WR exhibits an annual rainfall amount of 1754 mm (Liu and Han 2020). Under the circumstances of agricultural and industrial development, a great amount of factitious wastes were discharged directly or indirectly into river water, and a large number of cascade reservoirs were constructed along NR and WR (Yang et al. 2018). Cretaceous A-type and I-type granites (98–119 Ma) are predominantly underlain in JLJ River basin with a relatively small amount of Jurassic clastic rock and carbonate (Liu et al. 2019; Liu and Han 2020). A bit of sandstone is distributed along the estuary with no obvious existence of evaporites. There also exists some coal-bearing formations in the upper basin.

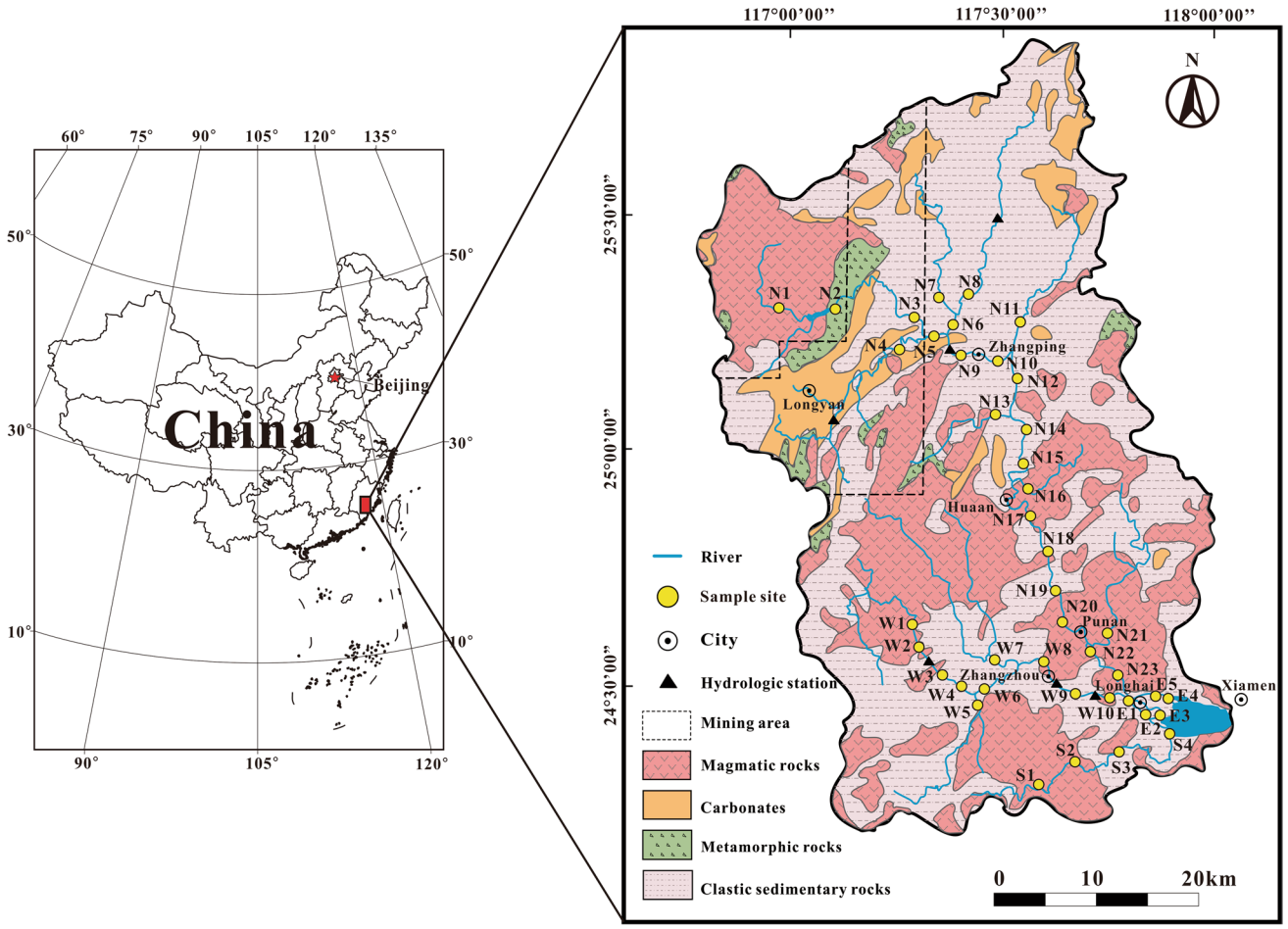


**Fig. 1** The location of sampling sites and geological map in JLJ River basin. Data of the lithology distribution were derived from the literatures (Li et al. 2019; Liu and Han 2020)

## Sampling and measurement

Water samples were collected at a depth of 15 cm from river center along the JLJ River in June 2017 (wet season), covering 42 sites in the name of N1–23, W1–10, S1–4, and E1–5 for NR, WR, SR, and the estuary (E), respectively (Fig. 1). Samples were stored in pre-cleaned high-density polyethylene (HDPE) bottles after rinsing, and samples for specified analysis were filtered through a 0.22-μm membrane (Millipore) in situ and stored in a 2-mL glass bottle. All containers were sealed and preserved at approximately 4℃ before measurement (Liu and Han 2020).

Water temperature, pH, EC (electric conductivity), and DO (dissolved oxygen) were measured in situ using a YSI water quality monitoring meter. Major cations ($Ca^{2+}$, $Mg^{2+}$, $K^{+}$, $Na^{+}$) and anions ($SO_4^{2-}$, $NO_3^{-}$, $Cl^{-}$) were derived by ion chromatography (DIONEX ICS-900) in the Institute of Geographic Sciences and Natural Resources Research, CAS. The relative standard deviations of major ions and Sr concentration were within ± 5%. The accuracy of analysis was determined by replicate samples and standard solutions, together with reagent and procedural blanks. Further details can be found in our previous work (Liu and Han 2020).

The pre-treatment and measurement of $\delta^{13}$C-DIC followed the method of previous research (Atekwana and Krishnamurthy 1998; Qin et al. 2020). In short, ~ 10 mL of each sample was injected into glass bottles with magnetic stir bars and 1-mL 85% phosphoric acid. After converting to $CO_2$ from DIC via chemical reaction, $CO_2$ was extracted into a vacuum line and passed through the $N_2$ cooled ethanol trap to separate $H_2O$. Next, $CO_2$ was transferred into a tube cryogenically for isotopic analysis. The $\delta^{13}$C-DIC of collected samples was performed relative to V-PDB (accuracy of ± 0.1‰) by a mass spectrometer (Finnigan MAT252). For the analysis of N and O isotopes in $NO_3^{-}$, samples were firstly filtered and stored in a freezer (< − 20 °C) to inhibit microbial activity and then determined via denitrifier method following previous study (Zeng et al. 2020b; Liu et al. 2021). Basically, after mixing with denitrifying bacteria in the vials, $NO_3^{-}$ was converted to $N_2O$ and

further purified for isotopic analysis. NaOH was also applied to remove other gases and prevent biological activities. The dual isotopes of nitrate ($\delta^{15}$N- and $\delta^{18}$O-$NO_3^-$) were derived relative to atmosphere $N_2$ (accuracy of ± 0.3‰) and V-SMOW (accuracy of ± 0.5‰), respectively. For $\delta^{34}$S analysis, the dissolved $SO_4^{2-}$ of water samples were converted to barium sulfate precipitation ($BaSO_4$) by adding 10% barium chloride solutions ($BaCl_2$). After enough resting time (50 h), samples were filtered through a 0.22-μm membrane to separate the precipitation and then calcined under 800 °C for nearly 40 min. The determination of S stable isotope ($\delta^{34}$S-$SO_4^{2-}$) was conducted using Finnigan Delta-C isotope IRMS, and the results were relative to V-CDT (Liu and Han 2020). Water samples for Sr isotopic analysis were dried directly on a hotplate at 90 °C and then treated with 2-mL concentrated $HNO_3$ to remove any organic material. Finally, the solutions were dried and completely dissolved in a 2-M HCl + 0.1 M HF mixture before chemical separation. The one-step separation procedure via AG50W-X12 resin can be found in our previous work (Li and Han 2021). After the column protocol, the samples were dried at 90 °C and re-dissolved in $HNO_3$ and then evaporated until dryness and dissolved in 2 vol% $HNO_3$ for measurement. The Sr isotopic analysis was performed by a Nu Plasma 3 multi-collector inductively coupled plasma mass spectrometer (MC-ICP-MS, Nu Instruments, UK) in the Surficial Environment and Hydrological Geochemistry Laboratory in China University of Geosciences (Beijing). Internally normalized $^{87}Sr/^{86}Sr$ ratios were derived to avoid mass bias using a constant $^{86}Sr/^{88}Sr$ value (0.1194) with the exponential law. Before running the isotope analytical sessions of samples, about 500 ppb standard solution of Sr (NIST SRM 987) was introduced into the plasma source, yielding an average value of 0.710299 ± 42 (2SD, $N = 14$) for evaluating the accuracy of the instrument.

**Table 1** Descriptive statistics of hydrochemical parameters, major ions, and multi-isotope compositions in JLJ River water ($n = 42$)

| Parameters | Units | Min | Max | Mean | SD |
|---|---|---|---|---|---|
| T | ℃ | 21.5 | 31.8 | 26.5 | 2.2 |
| pH | | 6.4 | 7.6 | 7.2 | 0.3 |
| EC | μS $cm^{-1}$ | 21 | 1602 | 160 | 242 |
| $Na^+$ | mg $L^{-1}$ | 1.5 | 189 | 10.7 | 30 |
| $K^+$ | mg $L^{-1}$ | 1.1 | 11.2 | 3.2 | 2.1 |
| $Ca^{2+}$ | mg $L^{-1}$ | 1.5 | 30 | 10.5 | 5.4 |
| $Mg^{2+}$ | mg $L^{-1}$ | 0.3 | 26.4 | 3.7 | 4.4 |
| $Cl^-$ | mg $L^{-1}$ | 0.9 | 110 | 8.1 | 17.1 |
| $NO_3^-$ | mg $L^{-1}$ | 0.9 | 69 | 10.5 | 11.1 |
| $SO_4^{2-}$ | mg $L^{-1}$ | 1.4 | 92 | 17.8 | 18.1 |
| $HCO_3^-$ | mg $L^{-1}$ | 7.5 | 49 | 22.1 | 9.2 |
| $SiO_2$ | mg $L^{-1}$ | 11.3 | 24.8 | 15.8 | 3.7 |
| TDS | mg $L^{-1}$ | 23 | 371 | 91 | 64 |
| $TZ^+$ | meq $L^{-1}$ | 0.2 | 11.7 | 1.4 | 1.8 |
| $TZ^-$ | meq $L^{-1}$ | 0.2 | 4.4 | 1.2 | 0.8 |
| Sr | μmol $L^{-1}$ | 0.084 | 1.307 | 0.490 | 0.2 |
| $^{87}Sr/^{86}Sr$ | | 0.7089 | 0.7164 | 0.7133 | 0.002 |
| $\delta^{13}$C-DIC | ‰ | −24.1 | −9.2 | −11.8 | 2.9 |
| $\delta^{15}$N-$NO_3^-$ | ‰ | 0.3 | 22.7 | 5.0 | 3.7 |
| $\delta^{18}$O-$NO_3^-$ | ‰ | −2.1 | 21.4 | 2.4 | 4.1 |
| $\delta^{34}$S-$SO_4^{2-}$ | ‰ | −9.3 | 18.0 | −0.4 | 6.7 |

$n$ indicates the number of samples. $TZ^+$ represents the total cationic charge; $TZ^-$ represents the total anionic charge; TDS represents the total dissolved solid; the data of $\delta^{34}$S-$SO_4^{2-}$ are referenced from our previous work (Liu and Han 2020)

## Results

### Physicochemical parameters

The statistics of hydrochemistry in JLJ River are presented in Table 1. Water temperature ($T$) had an average of 26.5℃ in the wet season, and river waters were slightly alkaline (average pH = 7.2). The TDS and EC values were 91 mg $L^{-1}$ and 160 μS $cm^{-1}$ in the wet season, respectively. Compared with other rivers in China, the mean TDS value (91 mg $L^{-1}$) was lower than that in Wujiang River (403 mg $L^{-1}$) (Lang et al. 2006) and Yellow River (502.5 mg $L^{-1}$) (Wang et al. 2012). The total cationic charge ($TZ^+ = 2Ca^{2+} + 2Mg^{2+} + K^+ + Na^+$) ranged from 0.2 to 11.7 meq $L^{-1}$, and $Ca^{2+}$ was the dominant cation in JLJ River, accounting for more than 50% of $TZ^+$. The anions were dominated by $HCO_3^-$. It is noteworthy that samples near the estuary and the lower reaches of SR displayed extremely high $Na^+$ and $Cl^-$ concentrations, which may due to seawater mixing around the estuary. To eliminate dilution effect, the elemental ratios of major ions were applied in the discussion section.

### Sr concentration and isotope compositions

The strontium concentration and its isotopic ratios of JLJ River are shown in Table S1 and Fig. 2. The Sr concentrations of JLJ River varied within a wide range from 0.084 to 1.307 μmol $L^{-1}$ (average 0.49 μmol $L^{-1}$), lower than the global mean value (0.89 μmol $L^{-1}$) (Palmer and Edmond 1992) and the Yangtze River (2.4 μmol $L^{-1}$) (Chetelat et al. 2008). The Sr concentrations of NR varied between 0.084 and 0.903 μmol $L^{-1}$ (average 0.458 μmol $L^{-1}$). For the two main tributaries, the Sr concentrations of WR varied from 0.356 to 1.022 μmol $L^{-1}$ (average 0.537 μmol $L^{-1}$), while SR varied between 0.399 and 0.482 μmol $L^{-1}$ (average 0.436 μmol $L^{-1}$). Sr concentration of NR slightly decreased along the river flow, whereas that of WR increased. There were no significant variations in SR.

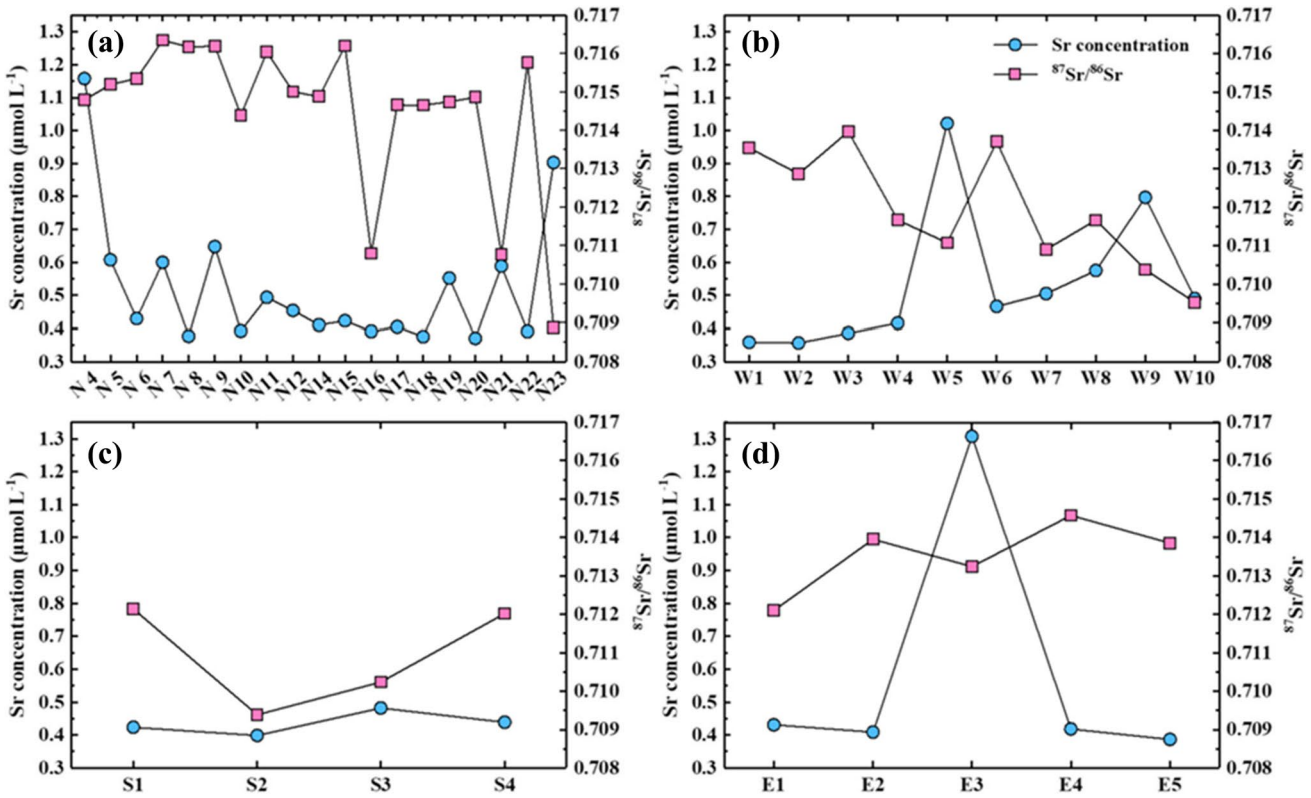


**Fig. 2** The spatial distribution patterns of Sr and its isotopic compositions in JLJ River basin

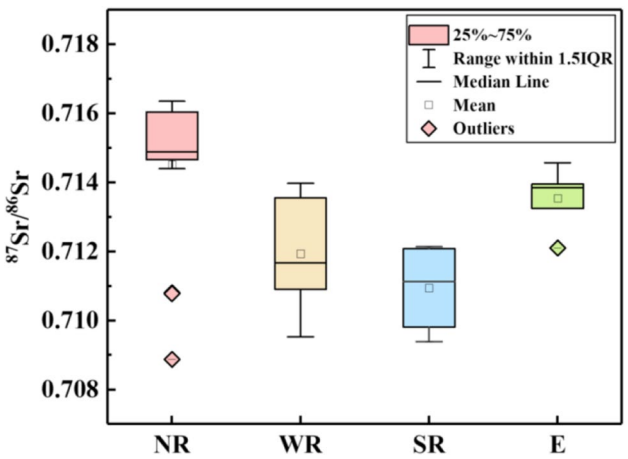


**Fig. 3** Box graph of Sr isotope ratios in JLJ mainstream, tributaries, and the estuary

The range of $^{87}Sr/^{86}Sr$ in JLJ River was shown in the box chart of Fig. 3. The $^{87}Sr/^{86}Sr$ ratios of the JLJ River water varied from 0.7089 to 0.7164 (average 0.7133), slightly higher than those in the previous research of Xijiang River (0.7085–0.7103) in southwest China (Wei et al. 2013), but lower than those in southern Himalayan rivers (0.7115–0.7822) (Bickle et al. 2003; Oliver et al. 2003; Singh et al. 2006). The mean value of $^{87}Sr/^{86}Sr$ is slightly higher than world average (0.7119) (Palmer and Edmond 1992). It should be noted in Fig. 2 that the Sr isotopic ratio of NR is slightly higher in comparison with WR and SR with an average of 0.7145. The decreasing of Sr isotopic ratios along with river flow may be attributed to the elevated surface runoff from other tributaries which provide waters with lower isotopic composition. The most dramatic fluctuation of $^{87}Sr/^{86}Sr$ occurred between N22 (0.7158) and N23 (0.7089) where WR and NR converged. A small drop in $^{87}Sr/^{86}Sr$ values was also recorded between sample N15 (0.7162) and N16 (0.7108), indicating the involvement of some local, yet unspecified, Sr sources with lower $^{87}Sr/^{86}Sr$. Nonetheless, since Sr concentration and discharge of SR were both lower than those of the estuary, the influence of SR on the Sr budget of the estuary is negligible.

## Multi-isotope compositions ($^{13}$C-DIC, $^{15}$N-$NO_3^-$, $^{18}$O-$NO_3^-$, $^{34}$S-$SO_4^{2-}$)

As shown in Table 1, measured $\delta^{13}$C-DIC in river waters ranged − 24.1‰ ~ − 9.2‰ (average − 11.8‰) in the wet season. The $\delta^{13}$C-DIC value of NR was slightly higher than that of WR and SR. The $\delta^{15}$N-$NO_3^-$ in river waters varied between 0.3 and 22.7‰ (average 5.0‰), and

$\delta^{18}O\text{-}NO_3^-$ varied − 2.1‰ ~ 21.4‰ (average 2.4‰). It is noteworthy that SR had $\delta^{15}N$ values three times higher than that in WR and NR, indicating different nitrate sources. The $\delta^{34}S\text{-}SO_4^{2-}$ of JLJ River ranged from − 9.3 to 18.0‰ with a mean value of − 0.4‰. An increasing trend in $\delta^{34}S\text{-}SO_4^{2-}$ values in NR was exhibited in the wet season, and the $\delta^{34}S\text{-}SO_4^{2-}$ signals in SR were higher than those in NR and WR. The average $\delta^{34}S\text{-}SO_4^{2-}$ value of JLJ River was much higher than that in Wujiang River (Li and Ji 2016; Liu and Han 2020).

## Discussion

### Sr isotope constraints on the implications of weathering

#### Sr variations and its implications

Low 1/Sr and $Si/TZ^+$ ratios of water samples in river basins could be connected to carbonate weathering, whereas high 1/Sr and $Si/TZ^+$ signature indicates the appearance of silicate weathering (Chen et al. 2020), since Sr has similar chemical properties to Ca as an alkaline earth metal and could replace it by isomorphism. 1/Sr exhibited a strong polarized trend against $Si/TZ^+$ in JLJ River basin (Fig. 4a), implying mixing end-members. It is noteworthy that N1, N2, N3, and N13 sites have extremely high 1/Sr and $Si/TZ^+$, while N4 has much lower 1/Sr and $Si/TZ^+$. Considering regional lithology (Fig. 1), N1–3 and N13 are generally silicate dominated, while N4 is carbonate dominated. Furthermore, samples W5, W9, and W10 exhibited lower 1/Sr and $Si/TZ^+$ as compared to other sites in WR, which may be attributed to the convergence of other small tributaries (W5) or the effect of cascade dams near hydrological stations (W9 and W10). In addition, a simple mixing relationship was also identified in the mainstream (NR) when plotting $^{87}Sr/^{86}Sr$ versus 1/Sr, but no obvious relationship was found in two tributaries (WR and SR) (Fig. 4b), indicating additional end-member contributions.

#### The end-member contributions on dissolved Sr

The determination of Sr end-member contributions is rather essential, since silicate-derived Sr flux could indicate the solid Earth $CO_2$ degassing process to alter coastal climate (Wang et al. 2007). The relative contributions of silicate and carbonate weathering can be derived from single end-member values by bedrock Na/Sr, Mg/Sr, and Ca/Sr ratios and Sr isotope ratios. The proportion of strontium isotopic compositions is calculated as follows (Wang et al. 2007):

$$\left(\frac{87_{Sr}}{86_{Sr}}\right)_{riv} = \left(\frac{87_{Sr}}{86_{Sr}}\right)_{rw} \times Sr_{rw} + \left(\frac{87_{Sr}}{86_{Sr}}\right)_{carb} \times Sr_{carb} + \left(\frac{87_{Sr}}{86_{Sr}}\right)_{ev} \times Sr_{ev} + \left(\frac{87_{Sr}}{86_{Sr}}\right)_{sil} \times Sr_{sil} \quad (1)$$

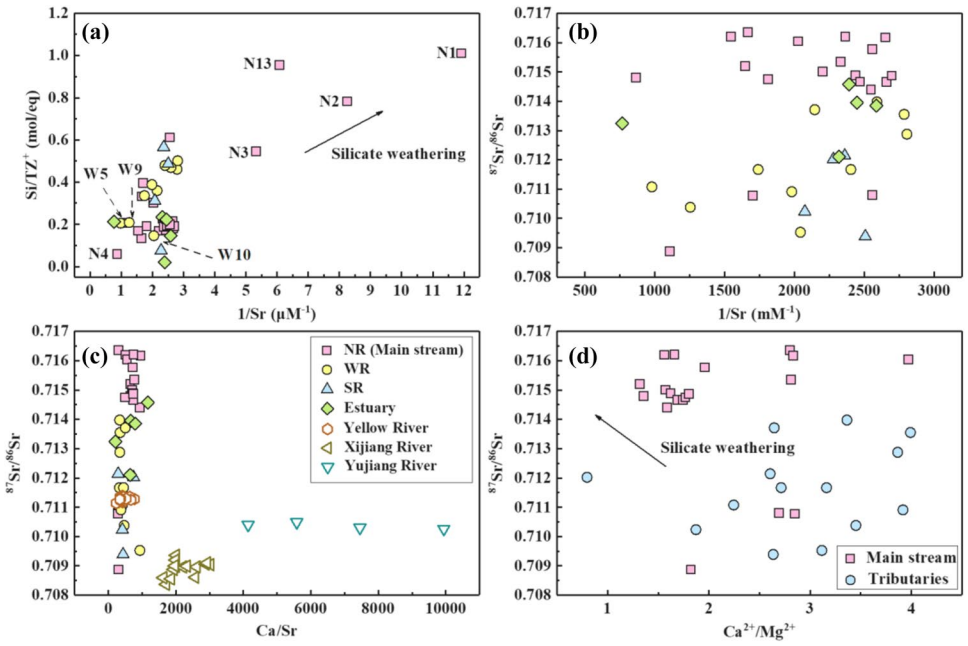


**Fig. 4** **a** 1/Sr versus $Si/TZ^+$ in each rivers and the estuary of JLJ River basin, **b** 1/Sr versus $^{87}Sr/^{86}Sr$ in each rivers and the estuary of JLJ River basin, **c** variations of $^{87}Sr/^{86}Sr$ versus Ca/Sr in JLJ River water, **d** $^{87}Sr/^{86}Sr$ versus $Ca^{2+}/Mg^{2+}$ molar ratios in JLJ River water. The isotopic and Ca/Mg data of Yellow River, Xijiang River, and Yujiang River were derived from literature (Wang et al. 2012)

Here, $(^{87}Sr/^{86}Sr)_{riv}$, $(^{87}Sr/^{86}Sr)_{rw}$, $(^{87}Sr/^{86}Sr)_{carb}$, $(^{87}Sr/^{86}Sr)_{ev}$, and $(^{87}Sr/^{86}Sr)_{sil}$ represent the $^{87}Sr/^{86}Sr$ isotopic ratios of river water, rainwater, carbonates, evaporates, and silicate rocks, respectively. $Sr_{rw}$, $Sr_{carb}$, $Sr_{ev}$, and $Sr_{sil}$ represent the relative contribution proportions of each end-member. Due to lack of $^{87}Sr/^{86}Sr$ data for carbonate and rainwater in JLJ River basin, we took the commonly referenced value of 0.709 in carbonate rivers and rainwater which is relatively closest to our study region (Han and Liu 2004). Since no evaporites appeared in JLJ River basin, the $(^{87}Sr/^{86}Sr)_{ev}$ were neglected. The $^{87}Sr/^{86}Sr$ ratio of 0.716 determined for continental crust was regarded as the Sr isotope composition of silicate reservoir (Capo et al. 1998). The formula can thus be simplified as:

$$\left(\frac{87_{Sr}}{86_{Sr}}\right)_{riv} = \left(Sr_{rw} + Sr_{carb}\right) \times 0.709 + Sr_{sil} \times 0.716 \quad (2)$$

Together with a simple mixing equation ($Sr_{rw} + Sr_{carb} + Sr_{sil} = 1$), the conclusion can be drawn that the mean proportion of carbonate weathering and rainwater accounts for 21% of total dissolved strontium in NR, while silicate weathering accounts for 79%. For two tributaries, the carbonate weathering and rainwater accounts for 58% of dissolved Sr in WR, whereas silicate weathering occupies 42%. And SR are 72% and 28%, respectively. Furthermore, the utilization of runoff coefficient in JLJ River basin can further discriminate the relative contribution of rainfall event from carbonates, since the rainfall events are generally coupled with hydrological responses in duration and runoff (Chen et al. 2022; Zeng et al. 2022). Thus, we took the monthly runoff coefficient of 0.53 in NR in the wet season as our reference value (Gao et al. 2018). The result shows that rainwater contributes 11% of total dissolved Sr in NR and carbonate weathering contributes the other 10%. The results generally indicate that the JLJ River basin is dominated by silicate rocks, while the lower proportions of silicate contribution to Sr isotopes in tributaries may be attributed to other potential chemical and geological impacts. Comparing to a recent research on the Mun River (the largest tributary in the pan-Mekong River basin) (Zhang et al. 2021), the silicate weathering contributions of the JLJ mainstream (79%) are nearly twice as high as that of the Mun River (37%) in Thailand, even though both two rivers are within the monsoon climate zone (Zeng et al. 2020a; Zhang et al. 2021). These variations are probably due to different regional geological conditions, since the Mun River basin is dominated by evaporite dissolution (Li et al. 2021), whereas the JLJ River is generally controlled by silicate weathering. However, considering the relatively insufficient sampling time, accuracy of laboratory analysis, and lack of rainwater measurement, the calculation results of this study may still exist with uncertainty to some extent and need further probabilistic investigations.

In order to determine Sr contributions from different rocks, molar ratios and the distribution of Sr isotope ratios were investigated in Fig. 4c. Most samples in JLJ River have lower Ca/Sr ratios and higher Sr isotope ratios as compared to Yellow River, Xijiang River, and Yujiang River, implying that dissolved Sr mainly originated from silicate weathering, whereas the contributions from carbonates are relatively small. The weathering proportions of silicate rocks can also be presented via plotting $^{87}Sr/^{86}Sr$ against $Ca^{2+}/Mg^{2+}$ (Fig. 4d), as the weathering products of silicate rocks have higher $^{87}Sr/^{86}Sr$ values (Krishnaswami et al. 1992) and generally lower $Ca^{2+}/Mg^{2+}$ ratios (Wei et al. 2013).

### Dissolved Sr flux and constraints on oceanic $^{87}Sr/^{86}Sr$

Quantitatively estimating the flux of dissolved strontium can provide insight into the impact of Sr flux to oceans, since JLJ River flows into the East China Sea through Xiamen Bay. In this study, the Sr flux of the JLJ River can be estimated by river discharge and the concentration of dissolved Sr. In addition, there is no obvious annual variation of river runoff based on historical data. The data of river discharge in JLJ main stream and its tributaries are derived from Liu et al. (Liu et al. 2019). Station Punan and Station Zhengdian were chosen to represent the mean river flux values in NR (520.83 $m^3\ s^{-1}$) and WR (224.92 $m^3\ s^{-1}$), respectively. Since there isn't any hydrological station in SR, the average total river flux value in the wet season (808.4 $m^3\ s^{-1}$) (Wang et al. 2013) was applied to subtract the value of NR and WR to obtain an estimate flux value of SR (62.65 $m^3\ s^{-1}$). We choose sites N23, W10, and S4 to represent the dissolved Sr concentrations of each river, since they are located at the most downstream channels without tidal influence. We assume the constancy of their concentrations during the sampling period. Therefore, the discharge-weight Sr concentration was calculated to be 0.066 mg $L^{-1}$, and the river output flux of dissolved Sr can be estimated in the wet season according to the Sr mass concentration of end-member input. The equation is simplified as:

$$F_j = Q_j \times C_j \quad (3)$$

**Table 2** Sr flux of JLJ in the wet season

| | | NR | WR | SR | Total |
|---|---|---|---|---|---|
| $Q_j$ | $m^3\ s^{-1}$ | 520.83 | 224.92 | 62.65 | 808.4 |
| $C_j$ | mg $L^{-1}$ | 0.079 | 0.043 | 0.039 | |
| $F_j$ | t/m | 106.65 | 25.07 | 6.33 | 138.1 |
| Percentage | % | 77 | 18 | 5 | 100 |
| Excess flux | t/m | | | | 0.63 |

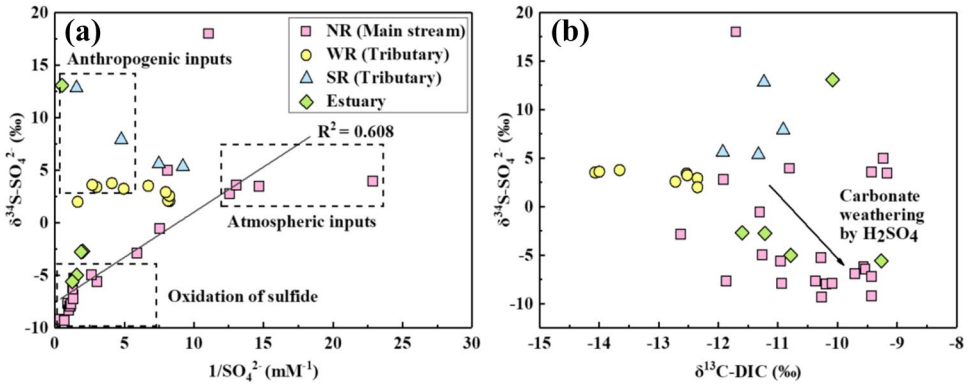


**Fig. 5** **a** Plots showing the mixing sources of sulfate in the JLJ River, **b** plotted $\delta^{34}S\text{-}SO_4^{2-}$ versus $\delta^{13}C$-DIC relationship in JLJ River basin

Here, $F_j$ represents the flux of dissolved Sr in river water (t/day or t/month); $Q_j$ represents the average discharge of river in the wet season ($m^3\ s^{-1}$); $C_j$ represents the average mass concentration end-member of dissolved Sr near the estuary (mg $L^{-1}$). The results demonstrate that the monthly flux of dissolved Sr from the JLJ River to the East China Sea is around 138.1 t $m^{-1}$ (Table 2) in total with the $^{87}Sr/^{86}Sr$ of 0.7135, in which the Sr flux of the main stream (NR) accounts for 77%, together with 18% and 5% from WR and SR, respectively. However, considering relatively insufficient sampling time and the accuracy of measurements, there is still some uncertainty in this calculation result which require further study.

The $^{87}Sr_{excess}$ flux (Wang et al. 2007) is a measurement of the relative flux of $^{87}Sr$ in excess of seawater strontium isotope composition (0.709) and can be derived from the following equation:

$$^{87}Sr_{excess}\,\text{flux} = \left(\frac{^{87}Sr}{^{86}Sr} - 0.709\right) \times \text{Total Sr}_{\text{flux}} \quad (4)$$

The calculated result of the JLJ River is around 0.63 t/m in the wet season. According to a recent research on the largest tributary of the Mekong River (Mun River, Thailand) (Zhang et al. 2021), its annual discharge ($2.6\times10^{10}$ $m^3$) and total basin area (71,060 $km^2$) are relatively comparable with the JLJ River in SW China (with a discharge of $1.4\times10^{10}$ $m^3$ and an area of 14,087 $km^2$). However, the $^{87}Sr$ in excess to the Mekong River (and finally to the Pacific Ocean) was estimated to be only 0.06 tons each year (Zhang et al. 2021), much less than that of the JLJ River. Considering relatively lower discharge and smaller basin area in our study region, these results obviously indicated the essential impact of JLJ River on the adjacent seawater Sr isotopic records.

## The impact of strong acids in weathering processes and C cycle

According to the Gibbs diagram of JLJ River presented in Fig. S1, it is obvious that most water samples exhibit the $Na^+/(Na^+ + Ca^{2+})$ ratio of 0.1 ~ 0.6 (average 0.3) and the $Cl^-/(Cl^- + HCO_3^-)$ ratio of 0.04 ~ 0.5 (average 0.2), indicating the primary dissolved ion source of rock weathering, rather than evaporation and precipitation. When providing sufficient sources of acids, sulfuric ($H_2SO_4$) and nitric ($HNO_3$) acids can be demonstrated as strong weathering agents (Perrin et al. 2008; Rao et al. 2017; Liu and Han 2020). Carbonate weathering by strong acids produces dissolved inorganic carbon (DIC) without consuming atmospheric $CO_2$. However, silicate weathering by strong acids plays a minor role on carbon cycle due to non-participation of carbon. As powerful tracers, $\delta^{34}S\text{-}SO_4^{2-}$ and dual isotopes of nitrogen have been widely applied in identifying sulfate and nitrogen sources (Li and Ji 2016; Liu et al. 2017) and, furthermore, the strong acid impacts on chemical weathering processes in coastal rivers.

### Sulfate sources based on S isotope

As a common sulfide mineral, pyrite usually occurs in sedimentary and igneous rocks (Spence and Telmer 2005) with the global contribution of 28% in riverine sulfide due to oxidative weathering (Burke et al. 2018; Ge et al. 2021). There exists a large magnetite mining area in NR basin, and its contact zone is abundant in sulfide. There are several small coal mines situated in Longyan City as well. The chemical reaction equations of carbonate and silicate dissolution by $H_2CO_3$ and $H_2SO_4$ agents are as follows:

$H_2CO_3$-carbonate weathering (CCW)

$$Ca_{1-x}Mg_xCO_3 + H_2CO_3 \rightarrow (1-x)Ca^{2+} + xMg^{2+} + 2HCO_3^- \quad (5)$$

$H_2SO_4$-carbonate weathering (SCW)

$$2Ca_{1-x}Mg_xCO_3 + H_2SO_4 \rightarrow 2(1-x)Ca^{2+} + 2xMg^{2+} + 2HCO_3^- + SO_4^{2-} \quad (6)$$

$H_2CO_3$-silicate weathering (CSW)

$$CaAl_2Si_2O_8 + 2CO_2 + 4H_2O \rightarrow Ca^{2+} + 2HCO_3^- + 2SiO_2 + 2Al(OH)_3 \quad (7)$$

$$NaAlSi_3O_8 + CO_2 + 2H_2O \rightarrow Na^+ + HCO_3^- + 3SiO_2 + Al(OH)_3 \quad (8)$$

$$KAlSi_3O_8 + CO_2 + 2H_2O \rightarrow K^+ + HCO_3^- + 3SiO_2 + Al(OH)_3 \quad (9)$$

$H_2SO_4$-silicate weathering (SSW)

$$CaAl_2Si_2O_8 + H_2SO_4 \rightarrow Ca^{2+} + SO_4^{2-} + 2SiO_2 + 2AlOOH \quad (10)$$

$$2NaAlSi_3O_8 + H_2SO_4 \longrightarrow 2Na^+ + SO_4^{2-} + 6SiO_2 + 2AlOOH \quad (11)$$

The major weathering products of carbonate and silicate weathering include $HCO_3^-$, $Ca^{2+}$, and $Mg^{2+}$, with a small number of $Na^+$ and $K^+$ when only $HCO_3^-$ is involved, so the equivalence ratio of $(Ca^{2+} + Mg^{2+} + Na^+ + K^+)/(HCO_3^-)$ should be close to 1. However, all river samples of JLJ River have larger ratios with the maximum of 11.31 and minimum of 1.24 (average 2.86), implying extra balance contributed by strong acids other than the original anions.

The natural sources of sulfate mainly include evaporite dissolution, atmospheric input, sulfide oxidation, and anthropogenic input. The effects of evaporite dissolution in JLJ are quite limited according to regional geologic setting (Fig. 1). Previous research have found the great impact on JLJ riverine chemical composition by anthropogenic activities, but the pollution source differentiates among NR, WR, and SR. Pollution source of NR is more related to coal mining and urban sewage (sulfide oxidation), whereas WR and SR are more related to urban sewage and anthropogenic agricultural wastes (nitrogen fertilizer) (Liu and Han 2020).

As shown in Fig. 5a, sulfate in JLJ River water came from anthropogenic inputs and the sulfide oxidation. The positive correlations between $\delta^{34}S$ and $1/SO_4^{2-}$ indicate mixing process from multiple sources. Mining activities lead to the oxidation of reduced sulfur and contribute more to the upper reach of the JLJ River, since the mining area is widely distributed in the upper part of the basin. Therefore, sulfuric acid produced from sulfide oxidation could become a useful agent of carbonate weathering. Figure 5b indicates the relationship between $\delta^{34}S$ and $\delta^{13}C$-DIC in the JLJ River. Enhanced $\delta^{13}C$-DIC values along with decreasing $\delta^{34}S$ values confirm the attendance of $H_2SO_4$ in the weathering process of carbonates, which is also in consistency with the findings from Li et al. (Li and Ji 2016).

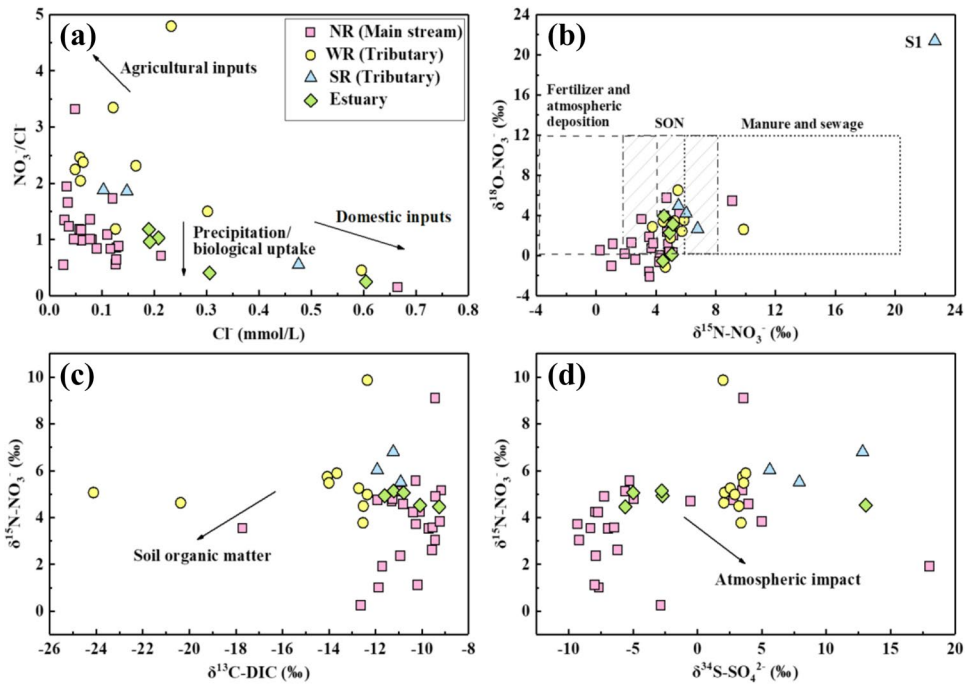


**Fig. 6** **a** $NO_3^-/Cl^-$ versus $Cl^-$ concentrations in JLJ River basin, **b** compositions of N–O isotopes from various sources in JLJ River basin, **c** variations of $\delta^{15}N\text{-}NO_3^-$ versus $\delta^{13}C$-DIC in JLJ River basin, **d** Variations of $\delta^{15}N\text{-}NO_3^-$ versus $\delta^{34}S\text{-}SO_4^{2-}$ in JLJ River basin

### The constraints of nitrate sources by N–O dual isotopes

The headwater of JLJ River flows through the karst area with complex geographical conditions. Cities and towns are densely distributed along the river with developed industry and cascade dams. In addition, the area of irrigation and agricultural fertilization accounts for a large proportion of land use in JLJ River basin. Therefore, the source of $NO_3^-$ in JLJ River is quite complex. Potential sources of nitrate mainly include precipitation, nitrogen fertilizer, urban sewage and manure, and soil organic nitrogen (SON). Lower $Cl^-$ concentrations and higher $NO_3^-/Cl^-$ ratios can be found in chemical fertilizers (Li and Ji 2016), whereas domestic inputs are generally on the contrary. Therefore, the variation of $NO_3^-/Cl^-$ is widely applied to distinguish the impact of anthropogenic activities. As shown in Fig. 6a, domestic inputs (manure and sewage) had less impact on river waters, while fertilizer and precipitation made greater contribution to nitrogen in JLJ River. Elevated $NO_3^-$ concentrations along with enhanced $SO_4^{2-}$ exhibited in the upper reach (N1–N5), demonstrating atmospheric deposition from mining area as a common source of $NO_3^-$ and $SO_4^{2-}$.

Stable isotope analysis is increasingly applied to investigate connectively in coastal aquatic-terrestrial ecosystems (Nakayama et al. 2018; Jiang et al. 2020). Dual isotopes of nitrate ($\delta^{15}N\text{-}NO_3^-$ and $\delta^{18}O\text{-}NO_3^-$) were plotted in Fig. 6b with typical source isotopic compositions to discriminate nitrite source, since different N sources have distinct N–O isotope signal (Kendall et al. 2007; Grabb et al. 2021; Jiang et al. 2021). As shown in Fig. 6b, $\delta^{15}N$ in most river samples generally falls into the range of three factors: nitrogen fertilizer/atmospheric deposition, manure/sewage, and SON (dominant input). Although precipitation has less impact on $NO_3^-$ in river water because of the lower $NO_3^-$ content of rainwater, larger runoff in the wet season would be regarded as an important transport process to carry more soil N and fertilizer into the river, which significantly affect the $NO_3^-$ content. It is noteworthy that an extremely high N–O isotopic composition appears in SR (sample S1), which may be attributed to the superimposed effects of urban waste water and denitrification. In addition, $\delta^{18}O\text{-}NO_3^-$ can be used to discriminate the sources of water nitrification and atmospheric deposition, since the $\delta^{18}O\text{-}NO_3^-$ of nitrification generally varies between − 10 and + 10‰, while that of atmospheric deposition was larger than 60‰ (Kendall et al. 2007; Wang et al. 2022). The $\delta^{18}O\text{-}NO_3^-$ compositions in most samples are in the range of ± 10‰, indicating the dominant process of nitrification.

In addition to nitrate isotopes, $\delta^{13}C$-DIC and $\delta^{34}S\text{-}SO_4^{2-}$ can also be applied to discriminate the sources and transport of riverine $NO_3^-$ (Li and Ji 2016). Under general circumstances, organic matters and/or sulfides contribute electrons in denitrification process ($NO_3^- \rightarrow N_2$ or $N_2O$), which could increase $\delta^{15}N$- and $\delta^{18}O\text{-}NO_3^-$ while simultaneously decrease $\delta^{13}C$-DIC and $\delta^{34}S\text{-}SO_4^{2-}$, since lighter isotopes are preferentially utilized (Kendall et al. 2007). The variation trend of $\delta^{15}N\text{-}NO_3^-$ versus $\delta^{13}C$-DIC plotted in Fig. 6c presented a slightly negative relationship, whereas the crossplots of $\delta^{15}N\text{-}NO_3^-$ versus $\delta^{34}S\text{-}SO_4^{2-}$ (Fig. 6d) exhibited no obvious relationships, indicating relatively limited impact of denitrification process on JLJ River basin during the sampling period. The depleted $\delta^{13}C$-DIC values and $\delta^{15}N\text{-}NO_3^-$ may be attributed to the oxidation of organic matters into C and N pools according to previous research (Li and Ji 2016). Nitric acid originated from SON oxidation can also occur in carbonate weathering; thus, the slight variation of $\delta^{15}N\text{-}NO_3^-$ and $\delta^{13}C$-DIC may be explained by carbonate dissolution with nitric acids produced from the nitrification process. Furthermore, the slightly increasing trend of $\delta^{15}N\text{-}NO_3^-$ and $\delta^{34}S\text{-}SO_4^{2-}$ may be attributed to deriving from atmospheric input, and a better explanation could be made if the typical isotope range of regional N and S from rainwater is accessible. The unclear relationships between $\delta^{15}N\text{-}NO_3^-$, $\delta^{13}C$-DIC, and $\delta^{34}S\text{-}SO_4^{2-}$ may also result from other mixing factors, such as precipitation intensity and the amount of riverine discharge during the wet season, which may be further elaborated in the future research.

### Carbonate weathering by strong acids: evidence from C isotope

Although granite bedrock dominates the lithology of JLJ River basin, the role of carbonate weathering still attracts significant attention, since carbonate rocks generally weather faster than silicate rocks (Gaillardet et al. 2018). Therefore, carbonate rocks and minerals are quite sensitive to various perturbations. JLJ River basin has a regional distribution of sulfide-associated iron deposits in the upper reach, corresponding with carbonate distribution. Therefore, the sulfuric acid contribution of carbonate weathering should be considered thoroughly.

As an important component of dissolved carbon transportation and main product of chemical weathering (Yin et al. 2020), DIC is composed of aqueous $CO_2$, $H_2CO_3$, $HCO_3^-$, and $CO_3^{2-}$ which could be identified by pH. Dissolved $HCO_3^-$ is the major component of DIC in the JLJ River and is equivalent to $\delta^{13}C$-DIC within the basin. Carbon evolution can thus be constrained by $\delta^{13}C$-DIC because of its relations to various DIC sources and biogeochemical processes, such as soil and atmospheric $CO_2$ (outgassing and exchange) and carbonate dissolution. To simplify the analysis, we assumed that riverine $\delta^{13}C$-DIC values have rather limited effects from photosynthesis process and $CO_2$ outgassing. Therefore, according to the weathering reactions with carbonate minerals, riverine

$Ca^{2+}$, $Mg^{2+}$, $HCO_3^-$, and $SO_4^{2-}$ (or $NO_3^-$) can be regarded as a mixing of carbonate weathering products. The contributions of $H_2CO_3$ and $H_2SO_4$ (or $HNO_3$) on carbonate weathering in JLJ River are represented as follows:

$$\left(\frac{HCO_3}{Ca+Mg}\right)_{theory} = \alpha_{sulf}\left(\frac{HCO_3}{Ca+Mg}\right)_{sulf} + \alpha_{carb}\left(\frac{HCO_3}{Ca+Mg}\right)_{carb} \quad (12)$$

$$\left(\frac{SO_4}{Ca+Mg}\right)_{theory} = \alpha_{sulf}\left(\frac{SO_4}{Ca+Mg}\right)_{sulf} + \alpha_{carb}\left(\frac{SO_4}{Ca+Mg}\right)_{carb} \quad (13)$$

$$\delta^{13}C_{theory}\left(\frac{HCO_3}{Ca+Mg}\right)_{theory} = \delta^{13}C_{sulf}\alpha_{sulf}\left(\frac{HCO_3}{Ca+Mg}\right)_{sulf} + \delta^{13}C_{carb}\alpha_{carb}\left(\frac{HCO_3}{Ca+Mg}\right)_{carb} \quad (14)$$

$$\alpha_{sulf} + \alpha_{carb} = 1 \quad (15)$$

where the $\alpha_{carb}$ ($\alpha_{sulf}$) denotes $Ca^{2+}$ ($Mg^{2+}$) proportions produced by $H_2CO_3$ ($H_2SO_4$) weathering. The chemical ratios and isotopic values with their errors of two weathering reactions are shown as follows:

(1) $H_2CO_3$-derived carbonate weathering:

$$HCO_3^-/(Ca^{2+}+Mg^{2+}) = 2$$

$$SO_4^{2-}/(Ca^{2+}+Mg^{2+}) = 0$$

$$SO_4^{2-}/(HCO_3^-) = 0$$

$$\delta^{13}C-DIC = -13 \pm 2‰$$

(2) $H_2SO_4$/$HNO_3$-derived carbonate weathering:

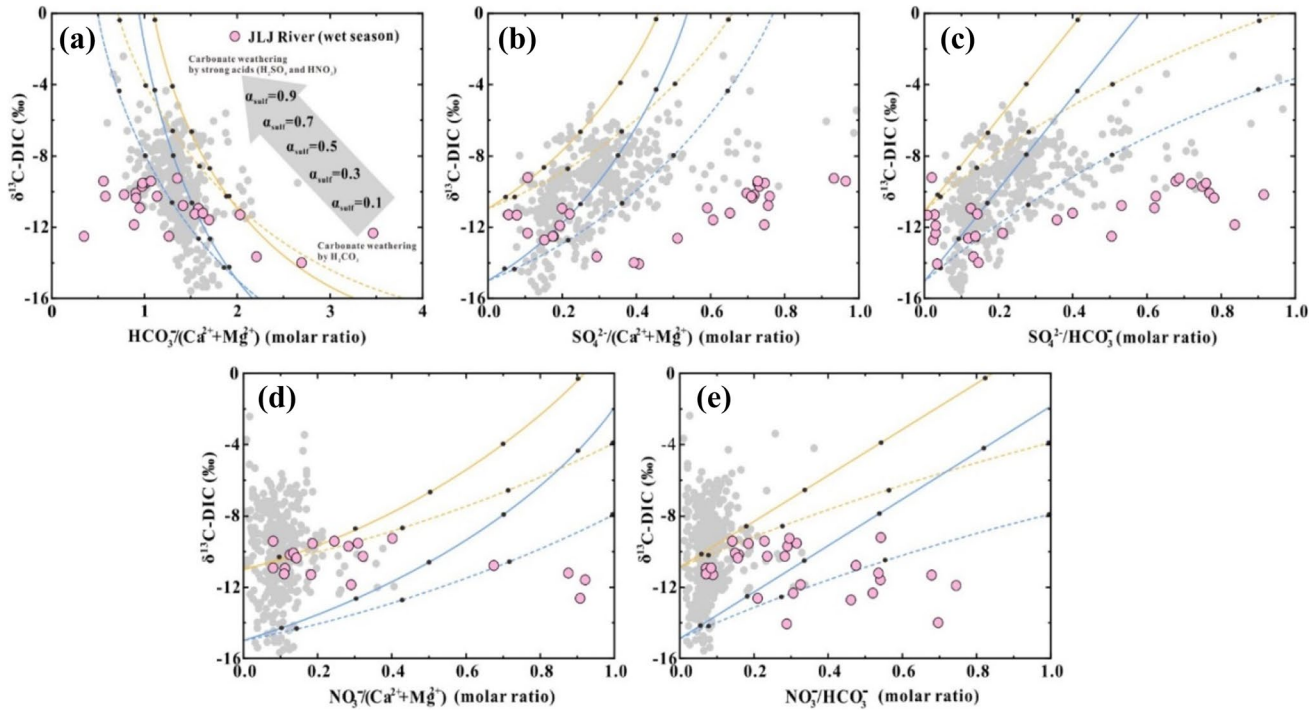


**Fig. 7** $\delta^{13}C$-DIC values versus molar ratios of $CO_3^-$, $SO_4^{2-}$, $NO_3^-$, and ($Ca^{2+}+Mg^{2+}$) in JLJ river waters. The anthropogenic and atmospheric inputs were corrected in the molar ratios. Yellow ($\delta^{13}C$-$DIC_{H2CO3\ weathering} = -11$ and $\delta^{13}C$-$DIC_{H2SO4\ weathering} = 2$) and blue ($\delta^{13}C$-$DIC_{H2CO3\ weathering} = -15$ and $\delta^{13}C$-$DIC_{H2SO4\ weathering} = -2$) solid lines represent the theoretical mixing lines between carbonate weathering triggered by $H_2CO_3$ and strong acids ($H_2SO_4$ and $HNO_3$). The dashed lines represent the mixture assuming 30% of ($Ca^{2+}+Mg^{2+}$) precipitation after carbonate dissolution. Gray solid points represent data from Xijiang River, Wujiang River, Houzhai River, and Beipanjiang River in literatures (Li et al. 2008, 2010a; Li and Ji 2016; Zhong et al. 2017, 2018)

$$HCO_3^-/(Ca^{2+}+Mg^{2+})=1$$

$$SO_4^{2-}/(Ca^{2+}+Mg^{2+})=0.5\ \ SO_4^{2-}/(HCO_3^-)=0.5$$

$$NO_3^-/(Ca^{2+}+Mg^{2+})=1\ \ NO_3^-/(HCO_3^-)=1$$

$$\delta^{13}C-DIC=0\pm2‰$$

This equation set has been solved by an inversion algorithm compatible to all parameters. The detailed information about this technique can be found in previous research (Spence and Telmer 2005; Li et al. 2008). The data was already corrected for atmospheric inputs and other end-members. As shown in Fig. 7, about one third of the data presented is located within the range of $H_2CO_3$ and $H_2SO_4/HNO_3$ weathering (Fig. 7b–7e), implying the contributions from strong acids. These results are also demonstrated by positive relationships between $\delta^{13}C$-DIC and $SO_4^{2-}/(Ca^{2+}+Mg^{2+})$.

The outranged data from the mixing lines probably indicate the predominant source of silicate weathering. In the JLJ River basin, the $HNO_3$-derived carbonate weathering makes more contribution to the whole weathering process than that of $H_2SO_4$ weathering, and the data displays a certain degree of deviation comparing to other researches on southwest China (gray dots in Fig. 7), reflecting the impact of different lithologies due to wide distribution of carbonate rocks in karst regions in southwest China. Moreover, according to previous research, the dominant local vegetation in JLJ River basin is $C_3$ plants with the mean $\delta^{13}C$ value of − 28.7‰, and the $\delta^{13}C$ of soil $CO_2$ should be − 24.3‰ after the correction of isotopic fractionation (Cerling et al. 1991). Samples N12, W1, and W2 in JLJ River all have relatively low $\delta^{13}C$ values (− 24.12‰ ~ − 17.72‰), indicating the potential impact of soil $CO_2$. Photosynthesis and $CO_2$ degassing could increase $\delta^{13}C$-DIC values to some extent (Li et al. 2010a; Li and Ji 2016). Therefore, our results of carbonate weathering contribution by $H_2SO_4$ and $HNO_3$ derived from mixing models and $\delta^{13}C$-DIC values may be overestimated on the total budget to some extent.

### Other potential constraints on coastal riverine weathering

Chemical weathering rates can be constrained by many factors, such as lithology, climate (temperature and precipitation), geomorphology, and tectonics (Gaillardet et al. 1999, 2018). According to our previous research about riverine hydrochemistry (Li et al. 2019), the calculated carbonate and silicate weathering rates of the JLJ River basin are $2.2\times10^5$ mol km$^{-2}$ and $3.7\times10^5$ mol km$^{-2}$ each year, respectively, and the real $CO_2$ consumption rate in JLJ River basin is 85.5% (or less) without considering the contribution of $H_2SO_4$ and $HNO_3$. The carbon sink $CO_2$ consumption may thus be overestimated due to the ignorance of strong acid effects on chemical weathering.

Previous study has indicated that the carbonates, highly sensitive to climate changes and human perturbations, generally weather 10–20 times faster than silicate rocks (Gaillardet et al. 2018). The consequently increased runoff with higher temperature would also change riverine solutes, resulting in the deviation of thermodynamic equilibrium in mineral dissolution. The relationship may also rely on the influence of soil moisture, soil $CO_2$, and far more agents. Although the mainstream exhibited rather limited impact of carbonate weathering on C cycle and climate change in a long-time scale (Ma), its fast perturbation to the carbon cycle at short-term scale is still remarkable (Xu et al. 2021). The process involved in terrestrial weathering would boost the coupling and interaction of basic elements on coastal riverine geochemistry, thus further affecting the adjacent marine ecosystems. However, the multi-isotope analysis of this study on coastal river system still has some limitations which may cause a certain impact on weathering calculations. Firstly, since the sampling was only done in the wet season, the seasonal variations of riverine solutes and water discharge may influence the analysis. Therefore, further comparison between two different seasons is necessary in such a monsoon-impacted coastal region in the future. Secondly, the uncertainty of input data may produce some deviation in the outcomes of end-member contribution, and this may be better illustrated via probabilistic methods like Bayesian (Ju et al. 2021) or Monte Carlo approach, which could be applied in future research.

## Conclusions

Dissolved Sr combined with multi-isotope analysis of the JLJ River was investigated to fingerprint coastal water sources and coupling interactions. The specific conclusions are as follows:

(1) The total cationic charge ($TZ^+$) ranged 0.2 ~ 11.7 meq $L^{-1}$ with the predominant $Ca^{2+}$ which accounted for > 50% of $TZ^+$, while the anions were dominated by $HCO_3^-$. The extremely high $Na^+$ and $Cl^-$ near the estuary indicated seawater mixing in such a coastal river. Sr concentrations of JLJ River varied 0.084 ~ 1.307 μmol

$L^{-1}$, and $^{87}Sr/^{86}Sr$ varied 0.7089 ~ 0.7164, slightly higher than world average.

(2) Dissolved Sr inputs are mainly affected by precipitation, weathering, and bedrocks. Silicate weathering accounts for 79% of dissolved Sr in JLJ mainstream, which is in line with lower Ca/Sr and $Ca^{2+}/Mg^{2+}$ ratios and higher $^{87}Sr/^{86}Sr$ values. The monthly Sr flux to the East China Sea is around 138.1 tons with the contribution of 77% in JLJ mainstream. The calculated $^{87}Sr_{excess}$ flux indicates an essential influence on the strontium isotope evolution in the ocean.

(3) $\delta^{13}C$ enhanced correspondingly to decreased $\delta^{34}S$, confirming the attendance of $H_2SO_4$ in carbonate weathering. Most $\delta^{18}O$ values exhibited within ± 10‰, indicating the dominant nitrification process. $\delta^{15}N$ presented slightly negative relationship with $\delta^{13}C$ and no obvious correlation with $\delta^{34}S$, indicating relatively limited impact of denitrification. The depleted $\delta^{13}C$ and $\delta^{15}N$ may be attributed to carbonate dissolution with nitric acids and the oxidation of organic matters into C and N pools. The multi-isotope approach demonstrated the involvement of strong acids in chemical weathering, which contributes more DIC to the upper reach of JLJ River. Due to larger runoff in the wet season, SON and fertilizer are washed out into coastal river and significantly affect $NO_3^-$ content. Therefore, the involvement of strong acids in weathering should be carefully considered in coastal environment.

**Supplementary Information** The online version contains supplementary material available at https://doi.org/10.1007/s11356-022-20223-z.

**Author contribution** **SZ:** Data curation, methodology, writing—original draft, and writing—review and editing. **GH:** Conceptualization, data curation, methodology, investigation, resources, writing—original draft, writing—review and editing, and funding acquisition. **JZ:** Data curation, methodology, writing—original draft, and writing—review and editing. **ML:** Methodology and investigation. **XL:** Methodology and investigation. **JL:** Methodology and investigation. All authors read and approved the final manuscript.

**Funding** This work was funded by the National Natural Science Foundation of China (No. 41661144029; 41325010).

**Data availability** All data generated or analyzed during this study are included in this published article and its supplementary information file.

## Declarations

**Ethics approval and consent to participate** Not applicable.

**Consent for publication** Not applicable.

**Competing interests** The authors declare no competing interests.

## References

Aravena R, Robertson WD (1998) Use of multiple isotope tracers to evaluate denitrification in ground water: study of nitrate from a large-flux septic system plume. Groundwater 36:975–982

Atekwana EA, Krishnamurthy R (1998) Seasonal variations of dissolved inorganic carbon and δ13C of surface waters: application of a modified gas evolution technique. J Hydrol 205:265–278

Bertrand G, Petelet-Giraud E, Cary L, Hirata R, Montenegro S, Paiva A, Mahlknecht J, Coelho V, Almeida C (2022) Delineating groundwater contamination risks in southern coastal metropoles through implementation of geochemical and socio-environmental data in decision-tree and geographical information system. Water Res 209:117877

Bickle MJ, Bunbury J, Chapman HJ, Harris NB, Fairchild IJ, Ahmad T (2003) Fluxes of Sr into the headwaters of the Ganges. Geochim Cosmochim Acta 67:2567–2584

Boral S, Peucker-Ehrenbrink B, Hemingway JD, Sen IS, Galy V, Fiske GJ (2021) Controls on short-term dissolved 87Sr/86Sr variations in large rivers: evidence from the Ganga-Brahmaputra. Earth Planet Sci Lett 566:116958

Burke A, Present TM, Paris G, Rae EC, Sandilands BH, Gaillardet J, Peucker-Ehrenbrink B, Fischer WW, McClelland JW, Spencer RG (2018) Sulfur isotopes in rivers: insights into global weathering budgets, pyrite oxidation, and the modern sulfur cycle. Earth Planet Sci Lett 496:168–177

Cao Y, Xuan Y, Tang C, Guan S, Peng Y (2020) Temporary and net sinks of atmospheric CO2 due to chemical weathering in subtropical catchment with mixing carbonate and silicate lithology. Biogeosciences 17:3875–3890

Capo RC, Stewart BW, Chadwick OA (1998) Strontium isotopes as tracers of ecosystem processes: theory and methods. Geoderma 82:197–225

Cerling TE, Solomon DK, Quade J, Bowman JR (1991) On the isotopic composition of carbon in soil carbon dioxide. Geochim Cosmochim Acta 55:3403–3405

Chen B-B, Li S-L, Pogge von Strandmann PAE, Sun J, Zhong J, Li C, Ma T-T, Xu S, Liu C-Q (2020) Ca isotope constraints on chemical weathering processes: evidence from headwater in the Changjiang River, China. Chem Geol 531:119341

Chen L, Beiyuan J, Hu W, Zhang Z, Duan C, Cui Q, Zhu X, He H, Huang X, Fang L (2022) Phytoremediation of potentially toxic elements (PTEs) contaminated soils using alfalfa (Medicago sativa L.): a comprehensive review. Chemosphere 293:133577

Chetelat B, Liu CQ, Zhao ZQ, Wang QL, Li SL, Li J, Wang BL (2008) Geochemistry of the dissolved load of the Changjiang Basin rivers: anthropogenic impacts and chemical weathering. Geochim Cosmochim Acta 72:4254–4277

Ding H, Liu C-Q, Zhao Z-Q, Li S-L, Lang Y-C, Li X-D, Hu J, Liu B-J (2017) Geochemistry of the dissolved loads of the Liao River basin in northeast China under anthropogenic pressure: chemical weathering and controlling factors. J Asian Earth Sci 138:657–671

Fan H, Huang H (2008) Response of coastal marine eco-environment to river fluxes into the sea: a case study of the Huanghe (Yellow) River mouth and adjacent waters. Mar Environ Res 65:378–387

Gaillardet J, Dupré B, Louvat P, Allegre C (1999) Global silicate weathering and CO2 consumption rates deduced from the chemistry of large rivers. Chem Geol 159:3–30

Gaillardet J, Calmels D, Romero-Mujalli G, Zakharova E, Hartmann J (2018) Global climate control on carbonate weathering intensity. Chem Geol 527:118762

Gao X, Chen N, Yu D, Wu Y, Huang B (2018) Hydrological controls on nitrogen (ammonium versus nitrate) fluxes from river to coast in a subtropical region: observation and modeling. J Environ Manage 213:382–391

Ge X, Wu Q, Wang Z, Gao S, Wang T (2021) Sulfur isotope and stoichiometry–based source identification of major ions and risk assessment in Chishui River Basin, Southwest China. Water 13:1231

Grabb KC, Ding S, Ning X, Liu SM, Qian B (2021) Characterizing the impact of Three Gorges Dam on the Changjiang (Yangtze River): a story of nitrogen biogeochemical cycling through the lens of nitrogen stable isotopes. Environ Res 195:110759

Han G, Liu C-Q (2004) Water geochemistry controlled by carbonate dissolution: a study of the river waters draining karst-dominated terrain, Guizhou Province, China. Chem Geol 204:1–21

Han G, Tang Y, Liu M, Van Zwieten L, Yang X, Yu C, Wang H, Song Z (2020) Carbon-nitrogen isotope coupling of soil organic matter in a karst region under land use change, Southwest China. Agric Ecosyst Environ 301:107027

Jiang H, Liu W, Zhang J, Zhou L, Zhou X, Pan K, Zhao T, Wang Y, Xu Z (2020) Spatiotemporal variations of nitrate sources and dynamics in a typical agricultural riverine system under monsoon climate. J Environ Sci 93:98–108

Jiang H, Zhang Q, Liu W, Zhang J, Zhao T, Xu Z (2021) Climatic and anthropogenic driving forces of the nitrogen cycling in a subtropical river basin. Environ Res 194:110721

Ju Y, Mahlknecht J, Lee K-K, Kaown D (2021) Bayesian approach for simultaneous recognition of contaminant sources in groundwater and surface water resources. Curr Opin Environ Sci Health 25:100321

Kendall C, Elliott EM, Wankel SD (2007) Tracing anthropogenic inputs of nitrogen to ecosystems. Stable Isotopes in Ecology and Environmental Science 2:375–449

Krishnaswami S, Trivedi J, Sarin M, Ramesh R, Sharma K (1992) Strontium isotopes and rubidium in the Ganga-Brahmaputra river system: weathering in the Himalaya, fluxes to the Bay of Bengal and contributions to the evolution of oceanic 87Sr/86Sr. Earth Planet Sci Lett 109:243–253

Lang Y-C, Liu C-Q, Zhao Z-Q, Li S-L, Han G-L (2006) Geochemistry of surface and ground water in Guiyang, China: water/rock interaction and pollution in a karst hydrological system. Appl Geochem 21:887–903

Li C, Ji H (2016) Chemical weathering and the role of sulfuric and nitric acids in carbonate weathering: isotopes (13C, 15N, 34S, and 18O) and chemical constraints. J Geophys Res Biogeosci 121:1288–1305

Li S-L, Calmels D, Han G, Gaillardet J, Liu C-Q (2008) Sulfuric acid as an agent of carbonate weathering constrained by δ13CDIC: examples from Southwest China. Earth Planet Sci Lett 270:189–199

Li S-L, Liu C-Q, Li J, Lang Y-C, Ding H, Li L (2010a) Geochemistry of dissolved inorganic carbon and carbonate weathering in a small typical karstic catchment of Southwest China: isotopic and chemical constraints. Chem Geol 277:301–309

Li S-L, Liu C-Q, Li J, Liu X, Chetelat B, Wang B, Wang F (2010b) Assessment of the sources of nitrate in the Changjiang River, China using a nitrogen and oxygen isotopic approach. Environ Sci Technol 44:1573–1578

Li X, Han G (2021) One-step chromatographic purification of K, Ca, and Sr from geological samples for high precision stable and radiogenic isotope analysis by MC-ICP-MS. J Anal at Spectrom 36:676–684

Li X, Han G, Liu M, Yang K, Liu J (2019) Hydro-geochemistry of the river water in the Jiulongjiang River Basin, Southeast China: implications of anthropogenic inputs and chemical weathering. Int J Environ Res Public Health 16:440

Li X, Han G, Liu M, Liu J, Zhang Q, Qu R (2021) Potassium and its isotope behaviour during chemical weathering in a tropical catchment affected by evaporite dissolution. Geochim Cosmochim Acta 316:105–121

Liu J, Han G (2020) Major ions and δ34SSO4 in Jiulongjiang River water: investigating the relationships between natural chemical weathering and human perturbations. Sci Total Environ 724:138208

Liu J, Han G, Liu X, Yang K, Li X, Liu M (2019) Examining the distribution and variation of dissolved carbon species and seasonal carbon exports within the Jiulongjiang River Basin (Southeast China). J Coastal Res 35:784–793

Liu J, Li S, Zhong J, Zhu X, Guo Q, Lang Y, Han X (2017) Sulfate sources constrained by sulfur and oxygen isotopic compositions in the upper reaches of the Xijiang River, China. Acta Geochimica 36:611–618

Liu W, Jiang H, Shi C, Zhao T, Liang C, Hu J, Xu Z (2016) Chemical and strontium isotopic characteristics of the rivers around the Badain Jaran Desert, northwest China: implication of river solute origin and chemical weathering. Environ Earth Sci 75:1–16

Liu X-L, Han G, Zeng J, Liu J, Li X-Q, Boeckx P (2021) The effects of clean energy production and urbanization on sources and transformation processes of nitrate in a subtropical river system: insights from the dual isotopes of nitrate and Bayesian model. J Clean Prod 325:129317

Mahlknecht J, Merchán D, Rosner M, Meixner A, Ledesma-Ruiz R (2017) Assessing seawater intrusion in an arid coastal aquifer under high anthropogenic influence using major constituents, Sr and B isotopes in groundwater. Sci Total Environ 587:282–295

Marchina C, Bianchini G, Knoeller K, Natali C, Pennisi M, Colombani N (2016) Natural and anthropogenic variations in the Po river waters (northern Italy): insights from a multi-isotope approach. Isot Environ Health Stud 52:649–672

Mora A, Mahlknecht J, Ledesma-Ruiz R, Sanford WE, Lesser LE (2020) Dynamics of major and trace elements during seawater intrusion in a coastal sedimentary aquifer impacted by anthropogenic activities. J Contam Hydrol 232:103653

Nakayama K, Maruya Y, Matsumoto K, Komai K, Kuwae T (2018) Nitrogen fluxes between the ocean and a river basin using stable isotope analysis. Estuar Coast Shelf Sci 212:286–293

Negrel P, Allègre CJ, Dupré B, Lewin E (1993) Erosion sources determined by inversion of major and trace element ratios and strontium isotopic ratios in river water: the Congo Basin case. Earth Planet Sci Lett 120:59–76

Oliver L, Harris N, Bickle M, Chapman H, Dise N, Horstwood M (2003) Silicate weathering rates decoupled from the 87Sr/86Sr ratio of the dissolved load during Himalayan erosion. Chem Geol 201:119–139

Otero N, Torrentó C, Soler A, Menció A, Mas-Pla J (2009) Monitoring groundwater nitrate attenuation in a regional system coupling hydrogeology with multi-isotopic methods: the case of Plana de Vic (Osona, Spain). Agr Ecosyst Environ 133:103–113

Palmer M, Edmond J (1989) The strontium isotope budget of the modern ocean. Earth Planet Sci Lett 92:11–26

Palmer M, Edmond J (1992) Controls over the strontium isotope composition of river water. Geochim Cosmochim Acta 56:2099–2111

Perrin A-S, Probst A, Probst J-L (2008) Impact of nitrogenous fertilizers on carbonate dissolution in small agricultural catchments: implications for weathering CO2 uptake at regional and global scales. Geochim Cosmochim Acta 72:3105–3123

Qin C, Li S-L, Waldron S, Yue F-J, Wang Z-J, Zhong J, Ding H, Liu C-Q (2020) High-frequency monitoring reveals how hydrochemistry and dissolved carbon respond to rainstorms at a karstic critical zone, Southwestern China. Sci Total Environ 714:136833

Rao W, Han G, Tan H, Jin K, Wang S, Chen T (2017) Chemical and Sr isotopic characteristics of rainwater on the Alxa Desert Plateau, North China: implication for air quality and ion sources. Atmos Res 193:163–172

Roy S, Gaillardet J, Allegre C (1999) Geochemistry of dissolved and suspended loads of the Seine river, France: anthropogenic impact, carbonate and silicate weathering. Geochim Cosmochim Acta 63:1277–1292

Singh SK, Kumar A, France-Lanord C (2006) Sr and 87Sr/86Sr in waters and sediments of the Brahmaputra river system: silicate weathering, CO2 consumption and Sr flux. Chem Geol 234:308–320

Spence J, Telmer K (2005) The role of sulfur in chemical weathering and atmospheric CO2 fluxes: evidence from major ions, δ13CDIC, and δ34SSO4 in rivers of the Canadian Cordillera. Geochim Cosmochim Acta 69:5441–5458

Torres-Martínez JA, Mora A, Mahlknecht J, Kaown D, Barceló D (2021) Determining nitrate and sulfate pollution sources and transformations in a coastal aquifer impacted by seawater intrusion—a multi-isotopic approach combined with self-organizing maps and a Bayesian mixing model. J Hazard Mater 417:126103

Tripathy GR, Singh SK (2010) Chemical erosion rates of river basins of the Ganga system in the Himalaya: reanalysis based on inversion of dissolved major ions, Sr, and 87Sr/86Sr. Geochem Geophys Geosyst 11:Q03013

Wang B, Lee X-Q, Yuan H-L, Zhou H, Cheng H-G, Cheng J-Z, Zhou Z-H, Xing Y, Fang B, Zhang L-K, Yang F (2012) Distinct patterns of chemical weathering in the drainage basins of the Huanghe and Xijiang River, China: evidence from chemical and Sr-isotopic compositions. J Asian Earth Sci 59:219–230

Wang ZL, Zhang J, Liu CQ (2007) Strontium isotopic compositions of dissolved and suspended loads from the main channel of the Yangtze River. Chemosphere 69:1081–1088

Wang D, Zheng Q, Hu J et al (2013) Jet-like features of Jiulongjiang River plume discharging into the west Taiwan Strait. Front Earth Sci 7:282–294

Wang Z-J, Yue F-J, Lu J, Wang Y-C, Qin C-Q, Ding H, Xue L-L, Li S-L (2022) New insight into the response and transport of nitrate in karst groundwater to rainfall events. Sci Total Environ 818:151727

Wei G, Ma J, Liu Y, Xie L, Lu W, Deng W, Ren Z, Zeng T, Yang Y (2013) Seasonal changes in the radiogenic and stable strontium isotopic composition of Xijiang River water: implications for chemical weathering. Chem Geol 343:67–75

Wu Q, Han G (2018) δ13CDIC tracing of dissolved inorganic carbon sources at Three Gorges Reservoir, China. Water Sci Technol 77:555–564

Xu S, Li S, Su J, Yue F, Zhong J, Chen S (2021) Oxidation of pyrite and reducing nitrogen fertilizer enhanced the carbon cycle by driving terrestrial chemical weathering. Sci Total Environ 768:144343

Yang K, Han G, Liu M, Li X, Liu J, Zhang Q (2018) Spatial and seasonal variation of O and H isotopes in the Jiulong River, Southeast China. Water 10:1677

Yin X, Lin Y, Liang C, Tao S, Wang L, Xu Y, Li Y (2020) Source and fate of dissolved inorganic carbon in Jiulong River, southeastern China. Estuar Coast Shelf Sci 246:107031

Zeng J, Han G (2020) Preliminary copper isotope study on particulate matter in Zhujiang River, southwest China: application for source identification. Ecotoxicol Environ Saf 198:110663

Zeng J, Han G, Yang K (2020) Assessment and sources of heavy metals in suspended particulate matter in a tropical catchment, northeast Thailand. J Clean Prod 265:121898

Zeng J, Han G, Zhang S, Liang B, Qu R, Liu M, Liu J (2022) Potentially toxic elements in cascade dams-influenced river originated from Tibetan Plateau. Environ Res 208:112716

Zeng J, Yue F-J, Li S-L, Wang Z-J, Qin C-Q, Wu Q-X, Xu S (2020) Agriculture driven nitrogen wet deposition in a karst catchment in southwest China. Agric Ecosyst Environ 294:106883

Zhang Q, Wang H (2020) Assessment of sources and transformation of nitrate in the alluvial-pluvial fan region of north China using a multi-isotope approach. J Environ Sci 89:9–22

Zhang S, Han G, Zeng J, Xiao X, Malem F (2021) A strontium and hydro-geochemical perspective on human impacted tributary of the Mekong River Basin: sources identification, fluxes, and CO2 consumption. Water 13:3137

Zhang X, Xu Z, Liu W, Moon S, Zhao T, Zhou X, Zhang J, Wu Y, Jiang H, Zhou L (2019) Hydro-geochemical and Sr isotope characteristics of the Yalong River Basin, Eastern Tibetan Plateau: implications for chemical weathering and controlling factors. Geochem Geophys Geosyst 20:1221–1239

Zhong J, Li S-L, Tao F, Yue F, Liu C-Q (2017) Sensitivity of chemical weathering and dissolved carbon dynamics to hydrological conditions in a typical karst river. Sci Rep 7:1–9

Zhong J, Li SL, Liu J, Ding H, Sun X, Xu S, Wang T, Ellam RM, Liu CQ (2018) Climate variability controls on CO2 consumption fluxes and carbon dynamics for monsoonal rivers: evidence from Xijiang River, Southwest China. J Geophys Res Biogeosci 123:2553–2567

Zieliński M, Dopieralska J, Belka Z, Walczak A, Siepak M, Jakubowicz M (2016) Sr isotope tracing of multiple water sources in a complex river system, Noteć River, central Poland. Sci Total Environ 548–549:307–316